Geoscience Frontiers 14 (2023) 101460

HOSTED BY

Contents lists available at ScienceDirect

Geoscience Frontiers

journal homepage: www.elsevier.com/locate/gsf

Research Paper

Earthquake-induced liquefaction hazard mapping at national-scale in Australia using deep learning techniques

Ratiranjan Jena [a], Biswajeet Pradhan [a,b,c,d,*], Mansour Almazroui [b], Mazen Assiri [b], Hyuck-Jin Park [c]

[a] Centre for Advanced Modelling and Geospatial Information Systems (CAMGIS), School of Civil and Environmental Engineering, Faculty of Engineering and Information Technology, University of Technology Sydney, Australia
[b] Center of Excellence for Climate Change Research, Department of Meteorology, King Abdulaziz University, Jeddah 21589, Saudi Arabia
[c] Department of Energy and Mineral Resources Engineering, Sejong University, Choongmu-gwan, 209 Neungdong-ro, Gwangjin-gu, Seoul 05006, Korea
[d] Earth Observation Centre, Institute of Climate Change, Universiti Kebangsaan Malaysia, 43600 UKM, Bangi, Selangor, Malaysia

ARTICLE INFO

Article history:
Received 23 March 2022
Revised 30 June 2022
Accepted 20 August 2022
Available online 27 August 2022
Handling Editor: M. Yoshida

Keywords:
Earthquake induced liquefaction
PSHA
Deep learning
GIS
Australia

ABSTRACT

Australia is a relatively stable continental region but not tectonically inert, having geological conditions that are susceptible to liquefaction when subjected to earthquake ground motion. Liquefaction hazard assessment for Australia was conducted because no Australian liquefaction maps that are based on modern AI techniques are currently available. In this study, several conditioning factors including Shear wave velocity (Vs30), clay content, soil water content, soil bulk density, soil thickness, soil pH, distance from river, slope and elevation were considered to estimate the liquefaction potential index (LPI). By considering the Probabilistic Seismic Hazard Assessment (PSHA) technique, peak ground acceleration (PGA) was derived for 50 yrs period (500 and 2500 yrs return period) in Australia. Firstly, liquefaction hazard index (LHI) (effects based on the size and depth of the liquefiable areas) was estimated by considering the LPI along with the 2% and 10% exceedance probability of earthquake hazard. Secondly, ground acceleration data from the Geoscience Australia projecting 2% and 10% exceedance rate of PGA for 50 yrs were used in this study to produce earthquake induced soil liquefaction hazard maps. Thirdly, deep neural networks (DNNs) were also exerted to estimate liquefaction hazard that can be reported as liquefaction hazard base maps for Australia with an accuracy of 94% and 93%, respectively. As per the results, very-high liquefaction hazard can be observed in Western and Southern Australia including some parts of Victoria. This research is the first ever country-scale study to be considered for soil liquefaction hazard in Australia using geospatial information in association with PSHA and deep learning techniques. This study used an earthquake design magnitude threshold of M_w 6 using the source model characterization. The resulting maps present the earthquake-triggered liquefaction hazard and are intending to establish a conceptual structure to guide more detailed investigations as may be required in the future. The limitations of deep learning models are complex and require huge data, knowledge on topology, parameters, and training method whereas PSHA follows few assumptions. The advantages deal with the reusability of model codes and its transferability to other similar study areas. This research aims to support stakeholders' on decision making for infrastructure investment, emergency planning and prioritisation of post-earthquake reconstruction projects.

1. Introduction

Liquefaction is a behaviour of soil, where strength reduction occurs on saturated soil because of an increase in pore pressure during earthquake ground shaking (Seed et al., 1964, 1983; Seed and Idriss, 1971; Chakrabortty et al., 2021). Liquefaction may involve lateral displacement, loss of bearing capacity, and uplift of engineering structures. The impact of earthquake induced liquefaction on society may be seen from the long history of such events, including billions of dollars in damage observed in Mexico 1985, Northridge 1994, Kobe 1995, Loma Prieta 1989, and most recently, Christchurch and Japan 2011. Studies conducted on infrastructure planning in Australia focused on the liquefaction geohazard, given that soils susceptible to liquefaction exist in that country. Although Australia is a low seismic hazard zone relative to

* Corresponding author.
E-mail address: Biswajeet.Pradhan@uts.edu.au (B. Pradhan).

https://doi.org/10.1016/j.gsf.2022.101460

other tectonically active areas of the world, the country nevertheless experienced four major liquefaction events that have been documented (Mote and Dismuke, 2011). In 1897, during an (M_s 6.5) earthquake near Beachport, South Australia, liquefaction was observed (Mote and Dismuke, 2011); also in the 1903 (Ml 5.3) earthquake in Warrnambool, Victoria (Mitchell and Moore, 2007). In 1968 and 1979 sand blows were observed in Meckering and Perth in Western Australia, followed by a M_s 6.8 and 6.1 earthquake, respectively (Clark et al., 2010). Liquefaction assessment methodology has been well described by Seed and Idriss (1971) and further refined over the last 40 years. For liquefaction hazard (temporal probability of liquefaction) assessments, the critical input parameters are cyclic stress ratio (CSR) and ground conditions, in order to estimate liquefaction susceptibility (spatial probability of liquefaction) and Cyclic Resistance Ratio (CRR) (Seed and Idriss, 1971).

Generally, liquefaction potential mapping (probability of an earthquake that may cause liquefaction) is conducted using Standard Penetration Test (SPT) based methods that can be split into several categories, such as semi-empirical traditional methods, cyclic resistance (Seed and Idriss, 1971; Bolton Seed et al., 1985), the critical SPT-N (State Infrastructure Commission, 1974), and the liquefaction safety factor method (Ishihara, 1977; Tatsuoka et al., 1980) and data-driven based machine and deep learning methods which include decision tree (Liu and Tesfamariam, 2012, artificial neural network (ANN) (Juang et al., 2000; Zhang and Goh, 2018), support vector machine (Goh and Goh, 2007) and logistic regression methods (Liao et al., 1988; Zhang et al., 2013; Zhang and Goh, 2016). Juang et al. (2000) developed a neural network model to generate an empirical equation based on a cone penetration test (CPT) for liquefaction study. Pal (2006) proposed a support vector machine (SVM) model to investigate the liquefaction potential based on CPT and SPT field data. Ramakrishnan et al. (2008) conducted a study on the liquefaction potential mapping of loose sediments using an ANN model that indicates the suitability of an ANN approach. Mughieda et al. (2009) presented ANN models to investigate the soil liquefaction potential on the basis of CPT data. Farrokhzad et al. (2012) developed the liquefaction microzonation for Babol City based on an ANN model. Lee and Chern (2013) prepared a liquefaction prediction map using an SVM-based approach. All the above-described soft computing approaches are efficient as compared to statistical methods, although they have some shortcomings including over-fitting, poor performance, slow convergence, and local minimum arrival. A literature review shows that all the liquefaction studies are at local scale and based on field-based investigations. Samui and Sitharam (2011) conducted case studies of soil susceptibility to liquefaction based on machine learning models. They successfully applied ANN and SVM models and predicted liquefaction potential using SPT and CSR data. Zhang et al. (2020) successfully applied a constrained back propagation neural network (C-BPNN) model for the determination of liquefaction potential using SPT data with global applicability. Zhu et al. (2015) developed two liquefaction models with geospatial variables that include PGA, shear-wave velocity, compound topographic index, and a normalized distance parameter. They estimated the first-order approximations of the liquefaction spatial extent for use in rapid response, loss estimation, and simulations. In another work, Zhu et al. (2017) proposed two models that offer enhanced performance over previous models. For global application, they updated the geospatial liquefaction model. The best-performing model based on receiver operating characteristics (ROC) curve in a coastal setting uses distance to the coast as a geospatial conditioning factor. However, the second model uses PGV, V_S30, water table depth, proximity to the water body, and precipitation in non-coastal regions as conditioning factors. The second model, according to the authors, is suitable for global implementation.

In a separate work, Karpouza et al. (2021) conducted a study on earthquake induced secondary effects using multi-criteria decision-making methods. Their study demonstrates the seismically active regions characterised by both mountainous terrain and coastal plain in Xerias drainage basin is useful for the joint evaluation of slope destabilization and soil liquefaction hazard caused by earthquake. Bozzoni et al. (2021) conducted a study in Europe on megazonation of earthquake-induced soil liquefaction hazard. A logistic regression based probabilistic prediction model was developed using geospatial predictors that include PGA, Vs30 and the compound topographic index. To validate the results obtained using logistic regression model, a liquefaction database in continental Europe was used. Lin et al. (2020) demonstrated a framework for liquefaction susceptibility and probability assessment for ten earthquake scenarios in highway network in New Zealand. The exposure to the earthquakes resulted in a 40% of liquefaction probability. Goh (1994) successfully applied ANN for a liquefaction susceptibility study. Seed and his colleagues (1964, 1971, 1983) developed a methodology on the basis of CSR and SPT along with PGA to assess the soil liquefaction potential. This method is now a standard use for liquefaction studies around the world. Liao et al. (1988) and Cetin et al. (2000) presented a probabilistic model to estimate the variability and uncertainty associated with the liquefaction problem.

In Australia, Mosavat et al. (2013) conducted a liquefaction risk mapping for road foundations in the Gold Coast Region. They conducted several case studies which found low liquefaction failure potential for the considered moment magnitudes. Collins et al. (2004) conducted paleoliquefaction studies in Australia to derive earthquake hazard estimates. From their research on paleoliquefaction areas, they revealed several natural drainage intersections, where liquefaction deposits spanning different generations were found. Mote and Dismuke (2011) produced a screening-level liquefaction hazard mapping for Australia. They explored the range of magnitudes of earthquakes for a liquefaction triggering study in Australia and produced liquefaction maps. Very little research has been conducted on liquefaction, and what has been done suffered from considering too few factors, improper methodology and poor datasets (Dismuke and Mote, 2012; Semple, 2013).

Extensive review of the aforementioned literature indicates that estimating the liquefaction potential index (LPI) is a complex geotechnical problem because of the diversified nature of the soils and the participation of many other factors that affect the occurrence of liquefaction. Most liquefaction potential studies were conducted at a local scale based on the SPT data (Mitchell and Moore, 2007; Karthikeyan et al., 2013; Mosavat et al., 2013; Lin et al., 2020). These are field-based liquefaction studies conducted at local scale without the benefit of any deep learning analysis. However, some studies considered site classification information for the earthquake hazard assessments (Mote and Dismuke, 2011; Dismuke and Mote, 2012; McPherson and Hall, 2013; Ameri et al., 2017). No liquefaction potential and hazard index estimation and mapping were conducted on a national scale for Australia. Until now, no liquefaction hazard map was developed for Australia using deep learning techniques. Therefore, further assessment is necessary to test the feasibility of mapping detailed zones of liquefaction potential. As a novelty, this is the first ever study in Australia on liquefaction potential and hazard index assessment that can be considered an essential contribution to future geotechnical designs. This study used the shear wave velocity Vs30 dataset for the site classification of different soils across Australia, and then applied this to the liquefaction potential mapping. The goals of this earthquake-induced liquefaction study are to: (i) estimate liquefaction potential and hazard index for Australia, (ii) generate a

liquefaction hazard base map for Australia for future reference, (iii) compare the results obtained based on three approaches. Alternatively, this map can be created by combining several regional-scale geotechnical and geological datasets in association with detailed borehole information. The advantages deal with the reusability of model codes and its transferability to other similar study areas. This research aims to support decision making on infrastructure investment, emergency planning and prioritisation of post-earthquake reconstruction projects. Deep learning models are complex and PSHA follows few assumptions in the current integrated approach. The structure of the paper is organized as follows: a brief introduction to the liquefaction hazard and a literature review are described in Section 1. The detailed information on study area geology and tectonics setting are described in Section 2. Similarly, Section 3 discusses data and methodology whereas results are presented in Section 4. Additionally, in Section 4, we discuss the possible rationale behind the findings. To the end, Section 5 concludes the work with limitations, drawbacks, and future research.

2. Geology and tectonics

The geology of Australia can be divided into several principal sections: the Archaean age cratonic shields, Proterozoic basins and fold belts, Phanerozoic meta-igneous rocks, and sedimentary basins (Fitzsimons, 2003). The average thickness of the Australian continental crust is 38 km, varying from 24 km to 59 km (Spec and Pap, 2003). Generally, the continental crust is characterised by Archaean, Proterozoic and Palaeozoic granites and gneisses. Many parts of the Australian landmass consist of a thin veneer of sedimentary basins up to 7 km thick (Spec and Pap, 2003). The largest groundwater system in Australia is the Great Artesian Basin (Lilley et al., 2003). The basin comprises of 20% of Australia and holds 65,000 million megalitres of water that covers Queensland, New South Wales, parts of the Northern and Southern territory (Lilley et al., 2003). In Australia, the lineament pattern trends parallel to the shear planes network originally drawn by Vening Meinesz for a shift of 70° of latitude along the 90° longitude meridian (Meinesz, 1947). Australia's recent earthquakes are restricted to intraplate geologic events, as the continent is stable and away from the plate boundary (Meinesz, 1947).

The evolution of the Australian continent occurred over five distinct time periods, namely: 3800–2100 Ma, 2100–1300 Ma, 1300–600 Ma, 600–160 Ma and 160 Ma to the current state (Fitzsimons, 2003). The Australian extended shelf is divided into shelf, slope, and deep ocean floor (Spec and Pap, 2003). Biogenic debris and carbonates can be found on the outer shelf and upper slope. Desertic sand, sandy clay and relict carbonate also found as surficial sediments. The geomorphological features such as shoreface, Hummocky inner and outer plain, depressions, bedrock and mounds can be found in the continental shelf and desertic features can be found as geomorphological features in Australia (Ollier, 1979). These geologic events are surrounded by several Proterozoic belts and basins, particularly the granulite gneiss and igneous rock, the Arunta Block of amphibolite and granites, Glengarry Basin, the Gascoyne Complex, and Bangemall Basin. The study area is presented in Fig. 1.

The amplitude, frequency and ground motions of earthquakes are influenced by the regolith material beneath the soil layer

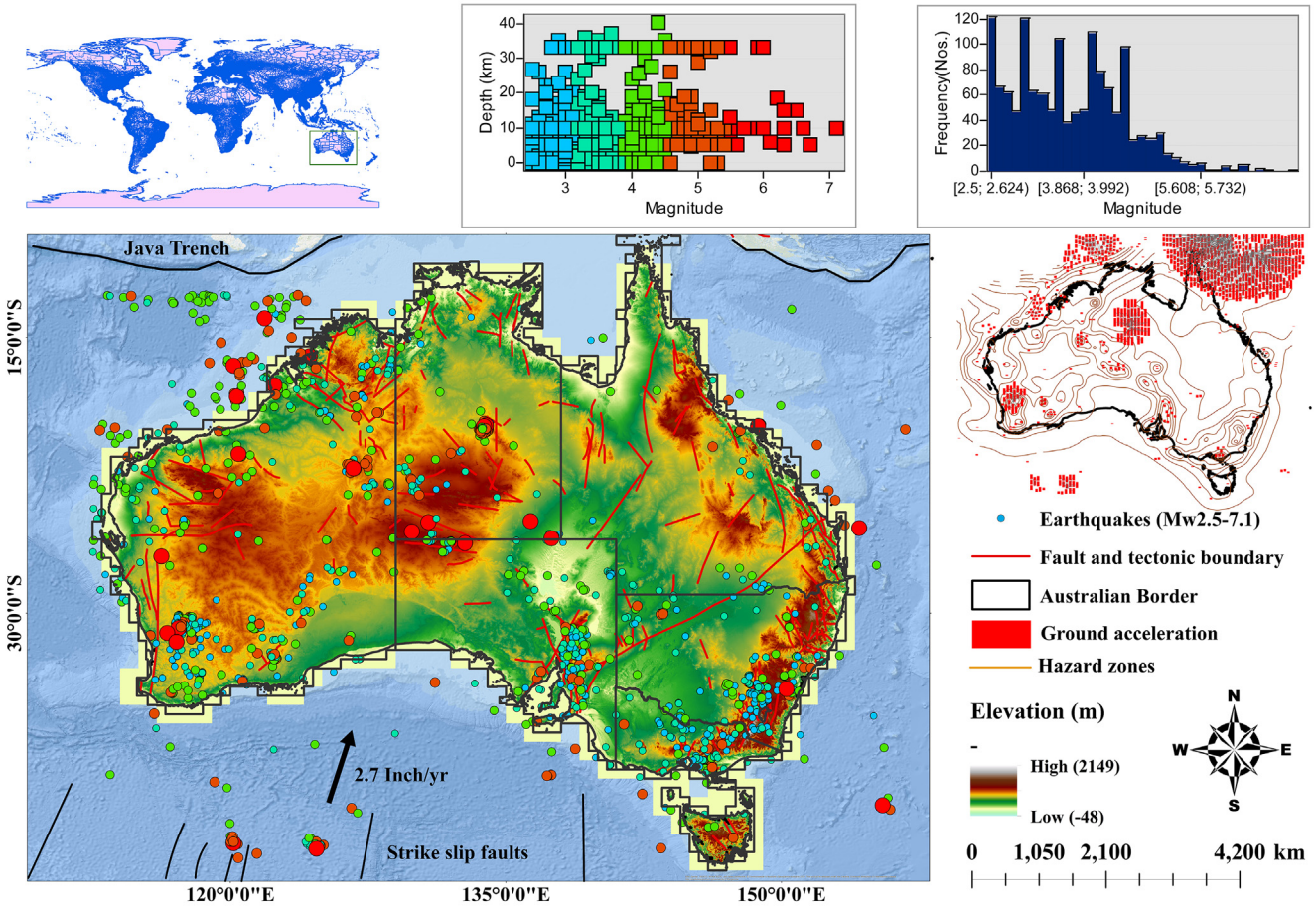

Fig. 1. Map of Australia showing state territories and earthquake hazard characteristics.

(Seed and Idriss, 1971). This particularly affects the occurrence and degree of damage to engineering structures and society (Seed and Idriss, 1971; Idriss, 1990). The Newcastle earthquake of 1989 demonstrated the spatial correlation between site conditions and building damage (Chandler et al., 1991). The site classification scheme was developed by Wills et al. (2000) validated for several Quaternary and unconsolidated deposits in several Australian sites such as Perth, Sydney, and Newcastle urban areas, using shear wave velocity of 30 m of soil (Vs30) data from previous geotechnical investigations. Vs30 information demonstrates the unit age and grain size influence on site classification (Tallett-Williams, 2017). Therefore, Australian soil characteristics are quite important for the Soil liquefaction study (Table 1). The soil map is depicted in Fig. 2A and groundwater system geomorphology and lithology are illustrated in Fig. 2B.

3. Data and methodology

The database included a base map for Australia, digitized at a scale of 1:10,000,000 including faults, inventory events, and various critical features collected from https://neotectonics.ga.gov.au/ . The geospatial dataset was collected directly from the database of Geoscience Australia. The hydro-geologic settings, lithology, groundwater movement and geomorphology information were also collected from the Geoscience Australia (https://www.ga.gov.au/) and were converted to thematic layers using geospatial information system (GIS) environment as described in Table 2. The analyses involved evaluating the surface lithology, soil types, soil characteristics and the surface water conditions, slope and elevation of the country (Fig. 3). The study implemented three approaches for the earthquake induced liquefaction hazard assessment. Firstly, this study estimated PGA using historical earthquake catalog through PSHA technique. Secondly, a multi-layer spatial analysis was conducted to estimate the GIS-based LPI for the country. For the LPI estimation, nine thematic layers were used as inputs in the multi-criteria decision-making model to assess the liquefaction potential zones. Here, Vs30 (29.9%), Clay content (21.0%), Water content (14.2%), and Bulk density (11.6%) were considered as the major contributing factors. The final hazard index was estimated by multiplying the PGA with LPI in the first approach. In the second approach, the PGA information was collected from Geoscience Australia which was directly multiplied by the LPI to estimate the hazard. In the third approach, PGA was involved as a factor to predict the top 10% of the previously published liquefaction hazard as a target using DNNs prediction model. Details about the data and the factors importance are provided in Table 2. The implementation of PSHA and deep learning are described in sub-section 3.1., 3.2. and 3.3., respectively.

Table 1
Soil data collected from Geoscience Australia based on Australian soil classification order.

ASC Order	Simplified description	Percentage of Australian soil	Amplification factor
Anthroposols	Soils resulting from human activities	No data	0
Calcarosols	Lime-rich soils with sandy or loamy textures that may become more clayey with depth	9.2	8–10
Chromosols	Neutral to alkaline soils with a sharp increase in texture with depth	3.0	3–6
Dermosols	Silicate clay, have loam to clay. Found in higher-rainfall coastal, delta and valleys	1.6	6–9
Ferrosols	Iron rich clay-loam to clay textures	0.8	<3
Hydrosols	Wet soils (sand and silt)	2.2	10–12
Kandosols	Sandy to loamy-surface soil, grading to porous sandy-clay subsoils	16.5	6–9
Kurosols	Acid soils texture increase with depth	1.0	3–6
Organosols	Organic soils such as peats	0.1	3
Podosols	Soils with accumulated organic matter, iron and aluminium	0.4	<3
Rudosols	Rudosols and Tenosols are poorly developed stony sand	14.0	<3
Sodosols	Soils with sodic subsoils	13.0	6–9
Tenosols	Slightly developed soils	26.3	<3
Vertosols	Cracking clays	11.5	<3

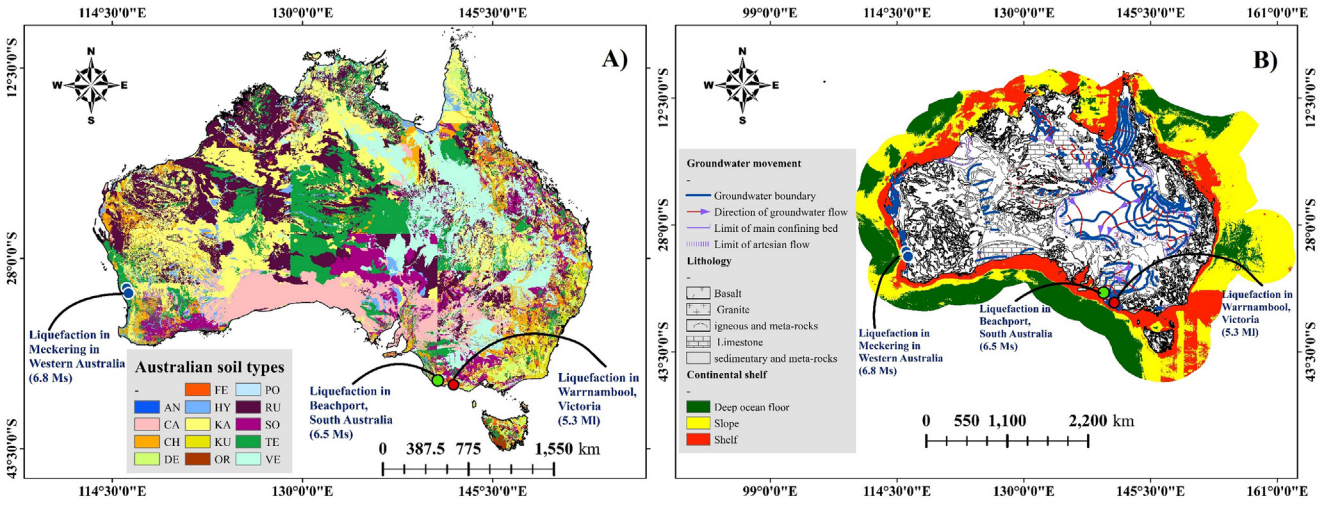

Fig. 2. (A) Liquefaction events plotted with soil map in Australia for different magnitude earthquakes. AN (Anthropologic), CA (Calcareous), CH (Chromosols), DE (Dermosols), FE (Ferrosols), HY (Hydrosols), KA (Kandosols), KU (Kurosols), OR (Organosols), PO (Podosols), RU (Rudosols), SO (Sodosols), TE (Tenosols), VE (Vertosols); (B) hydro-geological settings and geomorphology of Australia.

Table 2
Data sources, factors, threshold to liquefaction and characteristics used in this study.

Data	Factors	Source	Scale and resolution	Threshold to liquefaction	Description	References
Shear wave velocity (Vs30)	Vs30 site classification	USGS (https://earthquake.usgs.gov/data/vs30/)	30 arc-seconds (0.00833 degrees)	Vs30 < 295 m/s	Velocity decreases with decrease in rock/soil density that amplify the shear wave.	Castellaro et al., 2008
Soil properties	Clay contentSoil water contentBulk densitySoil thicknessSoil pH (Acidic or Basic characteristic)	Geoscience Australia (https://www.ga.gov.au/) Australian soil classification data	0.0025 degrees 0.0083 degrees	Clay Content < 10%–15% and Liquid Limit 0.9 × Liquid Limit, Bulk density < 1.6, Soil thickness < 30 m, Soil pH (4.5–6.5)	>40% clay content is not susceptible. Water content is a key parameter that partitions liquefiable and non-liquefiable silty/sandy soils. >1.6 bulk density means highly compacted soil. Silty sand and coarse grain sand comes under PH value of 4.5–6.5.	Andrews and Martin, 2000; Bray et al., 2004
Surface water	Distance from river	https://www.arcgis.com/	0.0025 degrees	Dis river < 3 km	More loose sediments can be found near river deposits/delta/pedeplain.	Wotherspoon et al., 2012; Chakrabortty et al., 2021
Digital elevation model	Slope Elevation	Earth explorer (USGS) and Geoscience Australia	0.0083 degrees	Slope < 2% Elevation < 10 m	Low slope and elevation are responsible for loose soil deposit which is susceptible for liquefaction.	Poulos et al., 1985;Olson and Stark, 2003
Historical event	PGA	USGS and Geoscience Australia	0.0083 degrees	Triggering threshold 6 M_w	Intraplate 6M_w event is a triggering event for soil liquefaction for such a huge continent. Low magnitude could not do that until unless the susceptible and event locations are close to each other.	

3.1. Probabilistic seismic hazard assessment

Probabilistic Seismic Hazard Assessment (PSHA) was employed to estimate earthquake hazard from a probabilistic perspective, as proposed by Cornell (1968). PSHA is an assumption-based analysis concerning earthquake magnitude (M) and distance (R). The overall steps of PSHA are presented in Fig. 4.

The basic equation for PSHA can be seen in the equation below by Cornell (1968).

$$\lambda(a > a^*) = \sum_{i=1}^{ns} v(m > m_0) \sum_{j=1}^{nm} \sum_{k=1}^{nr} P[a > a^* | m_j r_k] \times P[M_i = m_j] P[R_i = r_j] \quad (1)$$

Here, $\lambda(a > a^*)$ represents the Annual exceedance rate of a particular PGA. The annual occurrence rate of a 6 M_w earthquake can be presented as $v(m > m_0)$. The probability that the ground-motion parameter exceeds the level a^* for a magnitude of m (M_w 6) at a distance r is $P[a > a^* | m_j r_k]$. $P[M_i = m_j]$ represents the magnitude distribution function, and $P[R_i = r_j]$ is used as the distance distribution function. The analysis was conducted for 50 years, equivalent to return periods of 500 to 2500 years for the Australian continent. The PGA result of the country was further utilized for liquefaction hazard estimation corresponding to 500- and 2500-year return periods.

The PSHA steps are as follows.

(1) Data completeness analysis

The incompleteness of the earthquake data may cause overestimation or underestimation of parameters. To find out the complete earthquake catalogue in a particular period, the frequency of earthquakes for different magnitudes can be plotted against the calculated time from the last observation (Khan and Kumar, 2018). Visual observation of earthquakes in the study area provides information regarding completeness of data (Fig. 5A). Data can be considered as complete when a constant slope can be observed from the resulting graph (Khan and Kumar, 2018).

(2) Earthquake source modeling

Earthquake source modelling was conducted based on the source depth: 0–50 km for shallow crustal faults and subduction zones, 50–175 km, and 175–300 km for deep events. Each source category was assembled by area sources and a group of earthquakes from the same category can be found in each segment (Fig. 5B). The seismic parameters such as orientation, displacement, slip sense, depth, maximum magnitude range (M_{max}), rate of earthquake activity (λ), and ab-value as suggested by Gutenberg and Richter (1956) can be estimated from earthquake source modelling as presented in Table 3.

(3) Attenuation function selection

Parameters such as magnitude (M), intensity, and distance (R) can be understood from the attenuation function relationship (Joyner and Boore, 1981). The attenuation equation selection is determined by the mechanism of the earthquake, the distance from the epicentre and local soil conditions (ICOLD, 1989). In this study, the attenuation function referred to the Australian earthquake source and hazard, as described in Table 4. According to Nath and Thingbaijam (2012), the weights for the attenuation function for each source in the earthquake model were employed, as shown in the Table 4.

(4) Seismic hazard estimation

Seismic hazard was assessed by covering all Australia, including the nearest subduction zone. The PGA hazard results were estimated for 50 years, equivalent to 500 and 2500 years return periods and are presented in Fig. 5C and 5D which shows that the PGA varies from 0.032 to 0.48 g and 0.008 to 0.25 g, respectively.

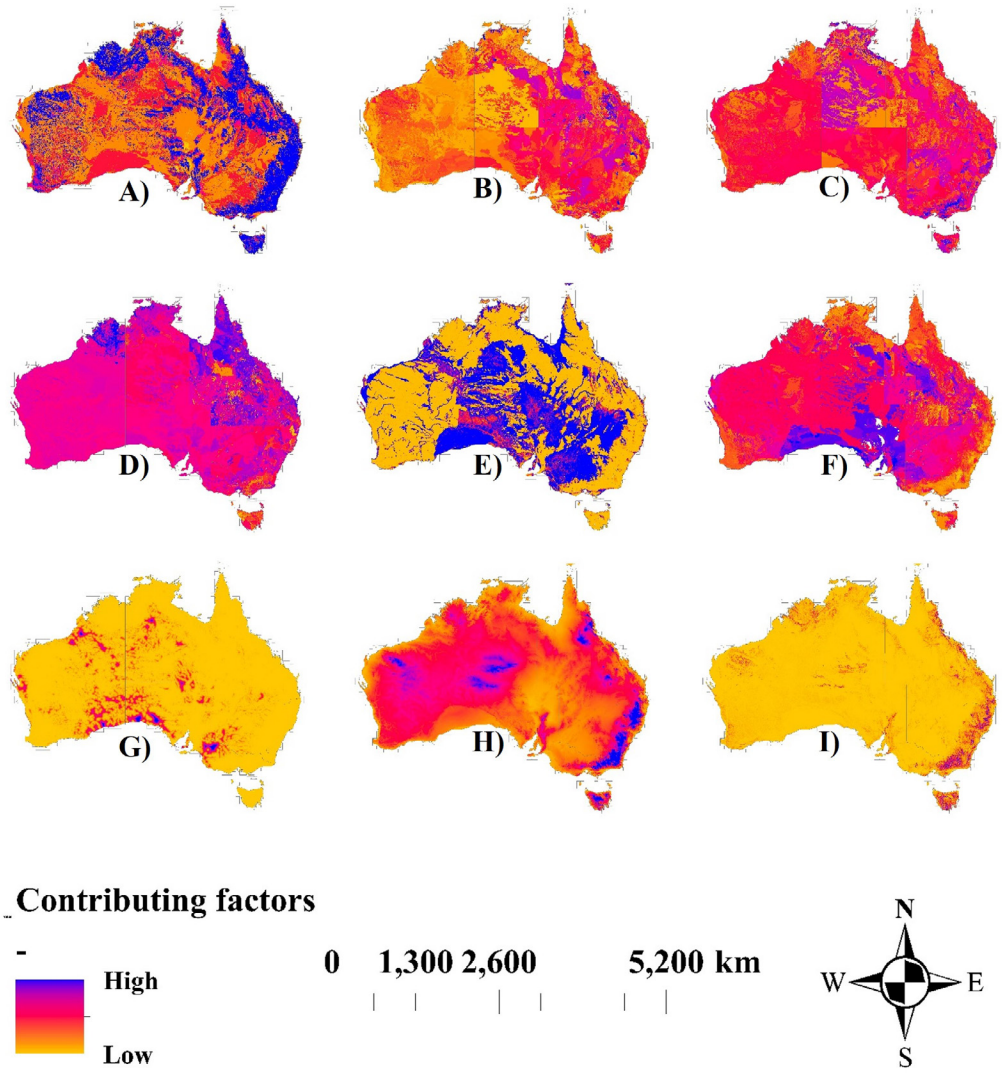

Fig. 3. Contributing factors to the soil liquefaction potential index estimation. A) Vs30 layer, B) clay content in soil, C) water content in soil, D) bulk density of soil, E) soil thickness, F) soil pH, G) distance from river, H) slope, and I) elevation.

3.2. Deep neural network architecture

Deep learning is a type of machine learning that includes statistical and predictive modelling (Zhang et al., 2017). This study employed deep neural networks (DNNs) for liquefaction hazard estimation. A series of fully connected dense layers construct the DNNs model that consider the attributes of every spectral and textural factor (Xu et al., 2014) for classification purposes, as elucidated in Fig. 6. The DNNs model successively computes output values where the network layers perform well for any given set of input features. The weighted sum is the main function in the hidden layer that includes output of every unit from the prior layer. The basic architecture of the applied DNNs model includes an input layer (L_{in}), an output layer (L_{out}), and hidden layers (L_h) that can be presented as $(h \in \{1, 2, \cdots, H\})$ between the input and output layers. A hidden layer (L_h) consists of several units that can be patterned as a vector $a_h \in R^{|L_h|}$, where $|L_h|$ indicates the total units in L_h. Hereafter, to parameterize every hidden layer, an activation function $f(\cdot)$, a bias vector $b_h \in R^{|L_h|}$, and a weight matrix $W_h \in R^{|L_{h_1}|*|L_h|}$, can be implemented. The units in L_h can be computed using the mathematical expression:

$$a_h = f(W_h^T a_{h-1} + b_h) \tag{2}$$

where the units a_0 originate from the compound feature vector in the input layer L_0, where $h = 1, 2, \cdots, H$. The activation function called rectified linear unit (ReLU) was employed in this study, and can be calculated as:

$$f(x) = max(0, x) \tag{3}$$

ReLU is a popular activation function used in deep learning (Glorot et al., 2011). This model employed a Softmax function for the classification prediction L_{out} followed by a_H estimation for the last hidden layer. Additionally, the model also used a loss function called

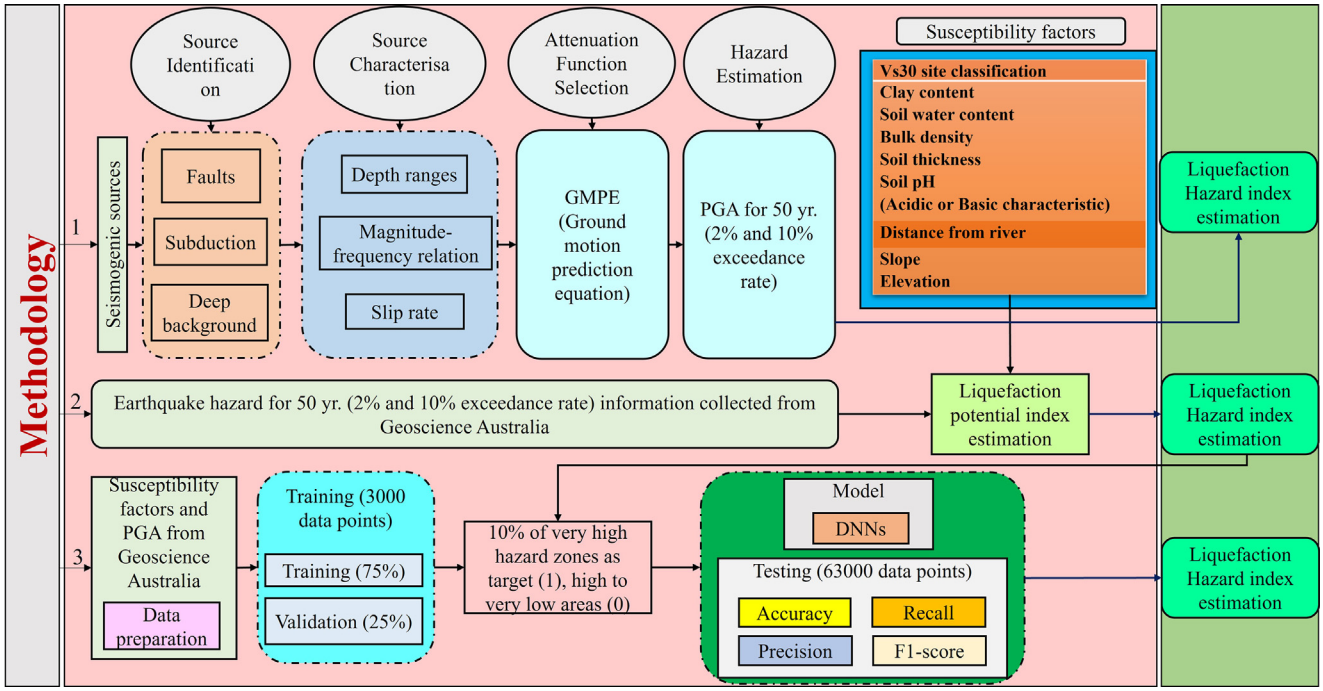

Fig. 4. Overall methodological flowchart for the earthquake induced soil liquefaction hazard index (LHI) estimation using three proposed approaches.

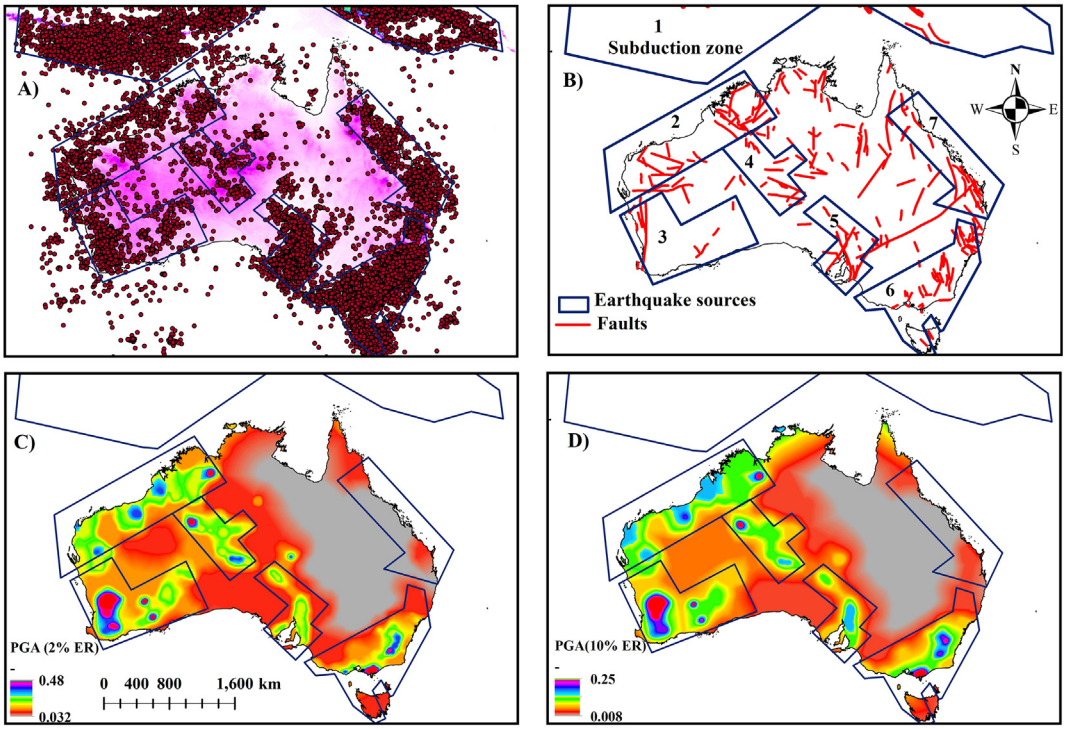

Fig. 5. (A) Data completeness and source identification, (B) source characterisation, (C) hazard estimation based on 2% exceedance rate (ER), and (D) 10% exceedance rate (ER) for 50 years.

categorical cross-entropy (CCE) to train the DNNs for classification (Murugan, 2018). The loss function for CCE can be estimated using the following formula:

$$L_{CCE}(g, f(I), \delta_1) = \sum_{i=1}^{S} \sum_{j=1}^{P} \sum_{c=1}^{C} -1\left(g_i^j = C\right) log l_c(I_i^j) \quad (4)$$

Here, the ground truth label is g_i^j, C is the number of classes, and the last dense layer output at the pixel I_i^j is $f(I_i^j)$. Moreover, δ_1 represents the network parameters, S is the batch size, the *jth* pixel in the *ith* patch is I_i^j, P is the pixels in each patch, and each class probability of the pixel I_i^j is $l_c(I_i^j)$ and is denoted as:

Table 3
Australian major faults characteristics and their future earthquake capacity. Data adopted from Quigley et al. (2006).

Fault (event)	Orientation (str/dip)(°)	Slickenlines (trd/pg)	Slip sense	D(m)	Timing	Depth FWsed (m)	FSR_{min} ($m/10^6$ y)	FSR_{ext} ($m/10^6$y)	SRL (km)	M_1 Prefrange	M_2
Wilkatana Fault northern (1)	330/46	33/113	R-LL	≥3.8	32–29 Ka[a]	93	>26	51	13.8	6.6 – 6.9	6.4
Wilkatana Fault northern (2)	330/46	33/113	R-LL	≥8.3–11.1	67–32 Ka[a]	93	>26	51	13.8	6.8 – 7.1	6.4
Knick point Fault	326/80	NA	R	≥ 4.2	≤ 12 Ka[a]	NA	NA	NA	13.8	6.6 – 6.9	6.4
Cobble Fault	355/69	NA	R	≥ 0.3	NA	NA	NA	NA	13.8	5.8–6.2	6.4
Wilkatana Fault southern	355/72	NA	R	≥ 6.1	≤ 80 Ka[a]	82	417	36	13.8	6.7–7.0	6.4
Burra Fault	161/36	35/252	R	≥ 3.8	≥ 83 Ka[a]	NA	NA	NA	39.9	NA	6.9
Mundi Mundi Fault	348/48	47/094	R	≥2.1	>59.3 Ka[a]	100[a]	>27	48	29.0	6.9–7.2	6.8

Slip sense: R, reverse; LL, left lateral.
Fault displacement (D).
FSR_{min} = Minimum fault slip rate.
FSR_{ext} = Extrapolated fault slip rate.
M_1 preferred magnitude range.
M_2 expected events.
[a] timing of fault movement.

Table 4
Attenuation function selection based on source characteristics and their weights.

Source	Attenuation function	Weights
Fault (0.5)	Boore-Atkinson NGA (2014)	0.13
	Campbell-Bozorgnia NGA (2014)	0.13
	Chiou and Youngs (2014)	0.10
	Gülerce et al. (2016)	0.10
Subduction zone (0.3)	Atkinson and Boore (2003) Intraslab rock and global source subduction	0.04
	Atkinson and Boore (2011)	0.12
	Abrahamson et al. (2016)	0.10
	Boore et al. (2014)	0.08
Deep Background (0.2)	Zhao et al. (2006) Geomatrix slab seismicity rock	0.10
	Atkinson and Boore (2003) interslab seismicity worldwide data region BC rock condition	0.10

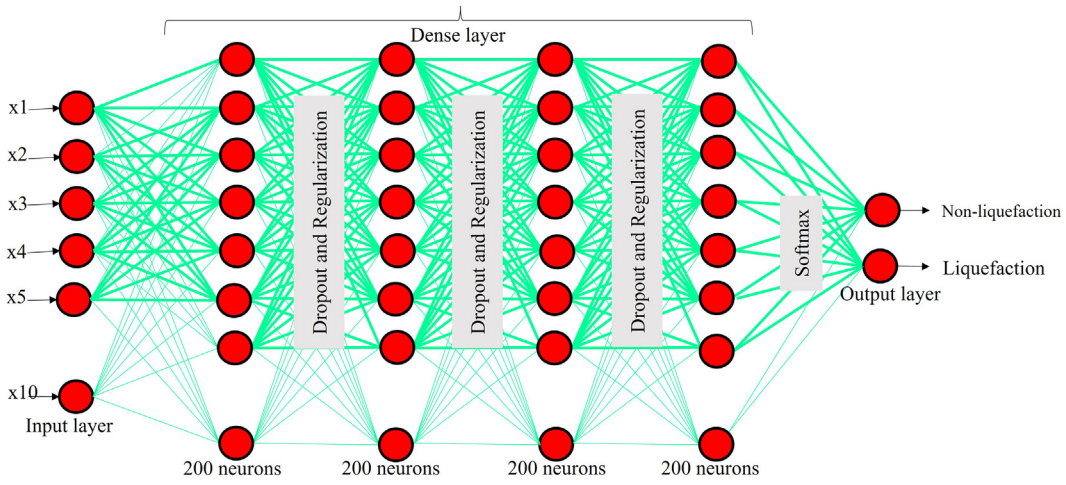

Fig. 6. The architecture of the proposed DNN model.

$$l_c\left(I_i^j\right) = \frac{\exp(f_c\left(I_i^j\right))}{\sum_{l=1}^{c} exp(f_l\left(I_i^j\right))} \quad (5)$$

The DNNs architecture is based on a multilayer feed-forward neural network and was applied using the Keras and TensorFlow libraries in python 3.5 for soil liquefaction mapping.

3.3. DNNs training and testing for liquefaction hazard

In this study, two datasets called the "training" and "testing" set are used for the DNNs model. To maintain an acceptable accuracy, dataset training was conducted, which highlighted the importance of data preparation (Jena et al., 2021). For training, the top 10% of the obtained liquefaction hazard map based on the second approach was used as a target (very-high) and the non-liquefaction hazards (moderate to very-low) were used to train DNNs. Thus, the model applied a strategy of using 75% of data for training, and 25% for validation of the liquefaction hazard prediction. The dataset according to that ratio of 75/25, while ratios of 70/30 and 80/20 are also suitable for small datasets (Jena et al., 2021). This study considers the liquefaction hazard map prepared by the Geoscience Australia as the basis for further analysis. Any scenario above the threshold of M_w 6 was used to conduct liquefac-

tion hazard mapping. The study employed 66,000 data points, out of which 63,000 points were for testing and 3000 for training. These data points represent both liquefaction and non-liquefaction points. The study achieved 94% and 93% accuracy with the testing dataset when generating 2% and 10% exceedance probabilities of liquefaction hazard. The four major liquefaction events in Australia and a map obtained by Dismuke and Mote (2012) were considered for validation purposes.

4. Results

4.1. Results of first approach

A liquefaction potential index (LPI) map was derived and is presented in Fig. 7. The major four significant factors were found to be Vs30 (29.9%), Clay content (21.0%), Water content (14.2%) and Bulk density of soil (11.6%), where the percentages are the weights obtained for the susceptibility index estimation. Based on the spatial distribution of conditioning factors of the liquefaction in the epicentral and surrounding areas, it can be inferred that the liquefaction potential is concentrated on Western Australia, but also includes some parts of central Australia. Spatial information of soil properties was used in order to analyse the liquefaction-prone soil for the country scale assessment. A very tiny part of South Australia is characterised as a very-high potential zone. A significant part of the northern territory is found to be susceptible to liquefaction. The time averaged shear wave velocity to 30 m depth of soil gives the most useful information regarding the site characteristics. The liquefaction potential was evaluated based on the classification developed by Iwasaki et al. (1984). In this study, very-high (>7), high (5–7), moderate (3–5), and low (0–3), ranges of the liquefaction potential index were estimated. Iwasaki et al. (1984) described in their study that no liquefaction phenomena can be expected when LPI is zero. When LPI ranges between 5 and 15, and 0 and 5, high and low potential can be anticipated, respectively. When the LPI exceeds 15, a very-high liquefaction potential is expected.

The earthquake hazard maps were estimated for 50 yrs based on the PSHA model. The PGA was estimated based on 2% (0.032–0.48 g) and 10% (0.008–0.25 g) annual exceedance rates. The liquefaction hazard map was derived based on LPI and PGA as shown in Fig. 8, which indicates that about 17% of Australia is highly hazardous, while about 45% is not hazardous, to an earthquake scenario above 6 M_w with PGA 0.48 g based on 50 yrs (Fig. 8A). Similarly, 14% of Australia is highly hazardous, while about 42% is not hazardous to an earthquake scenario of 6 M_w with PGA 0.25 g (Fig. 8B). The liquefaction hazard index (LHI) estimations, based on the 2% and 10% annual exceedance rates, were 0.032–1.920 and 0.008–0.5000, respectively. More importantly, it is evident that shallow groundwater tables and the increase in the thickness of soft soil deposits in the valley were more susceptible to liquefaction.

4.2. Results of second approach

The earthquake hazard information was collected from Geoscience Australia (GAH) for a 50 yr equivalent to 500 and 2500 yr return period, based on 2% and 10% annual exceedance rate. The PGA map portrays 2% (0–0.47 g) and 10% (0–0.18 g) annual exceedance rate. The liquefaction hazard map was derived from estimated LPI and PGA information as shown in Fig. 8. Based on the 2% exceedance rate of PGA the map demonstrates that about 16% of Australia is highly hazardous, while about 46% is not hazardous

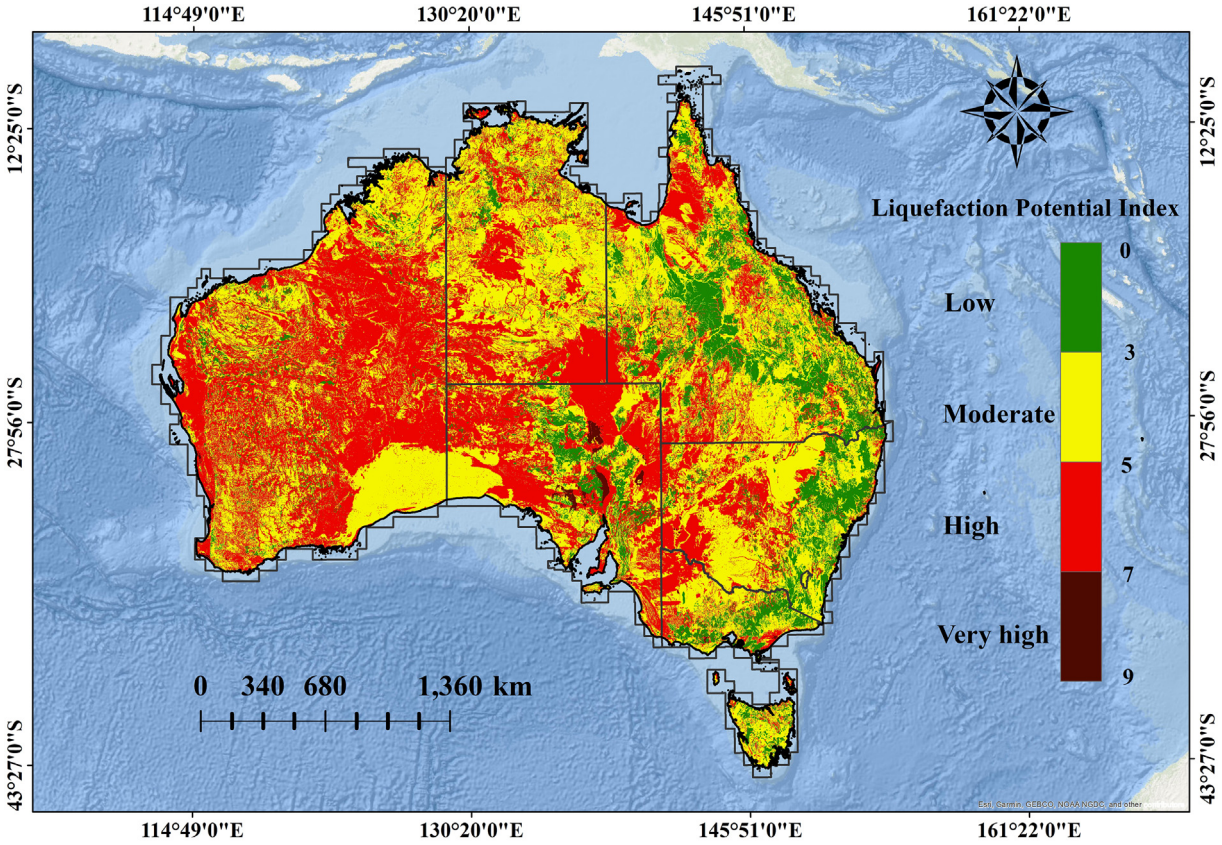

Fig. 7. Soil liquefaction potential index map for Australia.

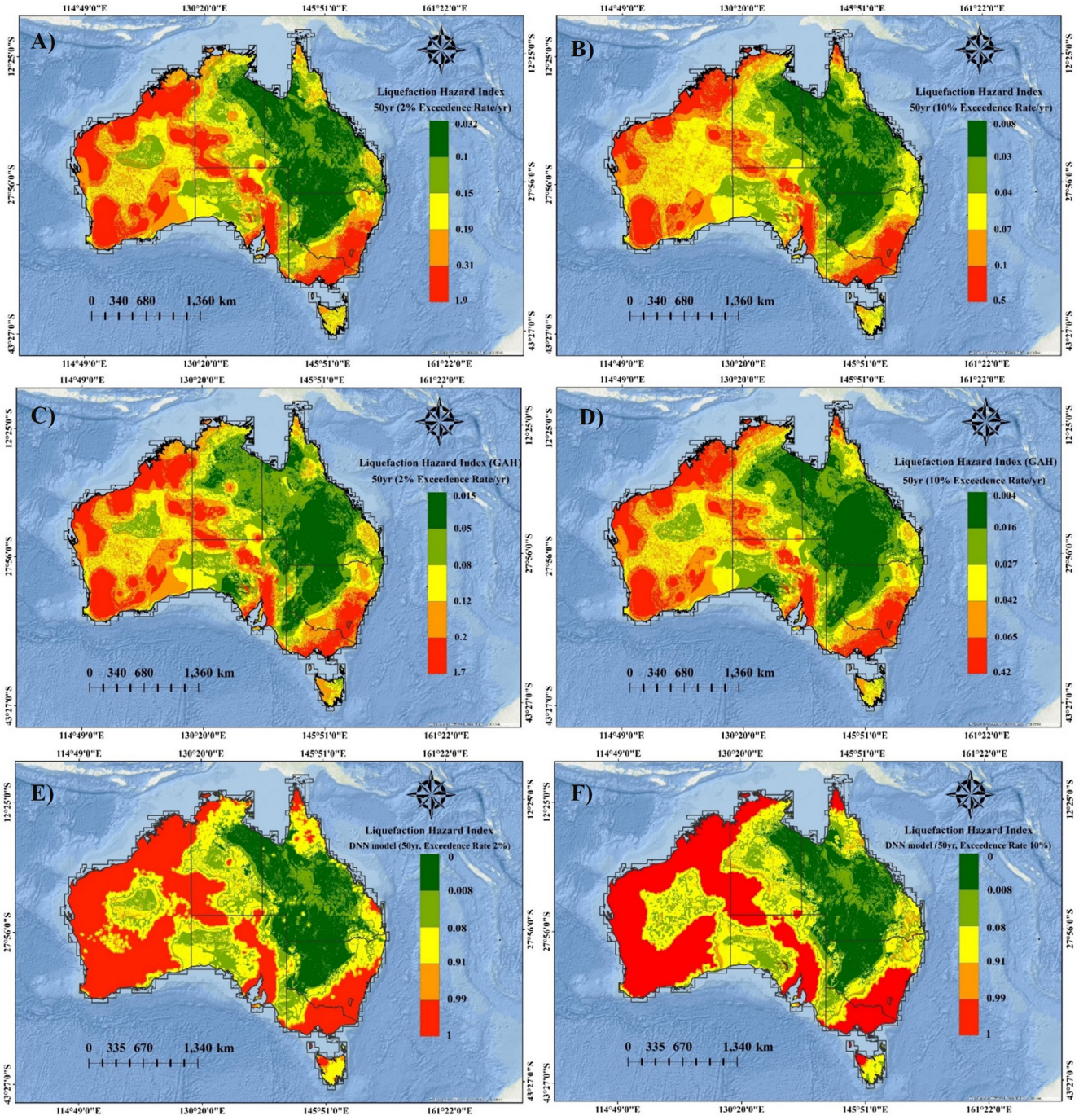

Fig. 8. Earthquake induced soil LHI maps for Australia. (A) Estimated LHI for 2% and (B) 10% probability of exceedance rate (ER), (C) Observed LHI for 2% and (D) 10% probability of exceedance rate (ER) based on Geoscience Australia's ground motion hazard information (GAH), (E) DNN model based LHI prediction for 2% and (F) 10% probability of exceedance rate (ER) based on top 10% very high hazard observed in (C) and (D).

to an earthquake scenario of 6 M_w, with PGA 0.47 g based on a 50 yr return period (Fig. 8C). Similarly, 15% of Australia is highly hazardous, while about 46.5% is not hazardous to an earthquake scenario of 6 M_w with PGA of 0.18 g (Fig. 8D). The LHI estimates based on the 2% and 10% annual exceedance rate of PGA, were 0.015–1.700 and 0.004–0.420, respectively. However, the liquefaction hazard based on GAH might be little higher than the PSHA based observed results. The classified maps showed red and orange zones as very high, and high liquefaction hazard zones, resp., while yellow represents moderate, and light and deep green areas show the low hazard zones.

4.3. Results of third approach

As mentioned earlier, the liquefaction susceptibility of any area mostly depends on geological conditions, soil properties, and ground motion characteristics (Trifunac, 2016). To sketch an overview of the spatial relationships between these factors and soil liquefaction, a parametric study was carried out using deep neural networks (DNNs) to predict the liquefaction hazard and show the influence of 2% and 10% probability exceedance rate on model output. The earthquake hazard of Australia (GAH) for a 50 yr period based on 2% and 10% annual exceedance rate was used along with

9 conditioning factors. The DNNs model predicted the liquefaction hazard location for 2% and 10% probability exceedance rate with an accuracy of 94% (Fig. 9A and B) and 93% (Fig. 9C and D), respectively. For the target, the top 10% of high liquefaction hazard areas were considered, as generated from PGA information from Geoscience Australia. Based on the 2% exceedance rate the map reveals that approximately 19% of Australia is highly hazardous to liquefaction, while about 45% is not hazardous, given an earthquake scenario of 6 M_w with PGA of 0.47 g based on a 50 yr period (Fig. 8E). Similarly, based on the 10% exceedance rate, 20% of Australia is highly hazardous, while about 45.5% is not hazardous to an earthquake scenario of 6 M_w with PGA of 0.18 g (Fig. 8F). The LHI based on the DNNs model was estimated at 2% and 10% annual exceedance rate of PGA, and ranged between 0 and 1. It shows that reasonable results can be achieved in this study with DNNs.

4.4. Comparative assessment among three approaches

Comparison of PSHA based liquefaction hazard, Geoscience Australia's PGA information-based liquefaction hazard and DNNs model based LHI has been presented. Results obtained by the three methods are very similar. As can be seen in Fig. 9, the prediction accuracy for DNNs is good and can be used as a preliminary basis for estimating liquefaction hazard in Australia. The DNNs model-based prediction classification results are shown in Table 5 for 2% and 10% probability of ER, respectively. The results are quite close to each other. Therefore, it is hard to interpret which result surpasses the other two results. Thus, it can be accepted that all the results could be reliable in earthquake-induced liquefaction hazard mapping.

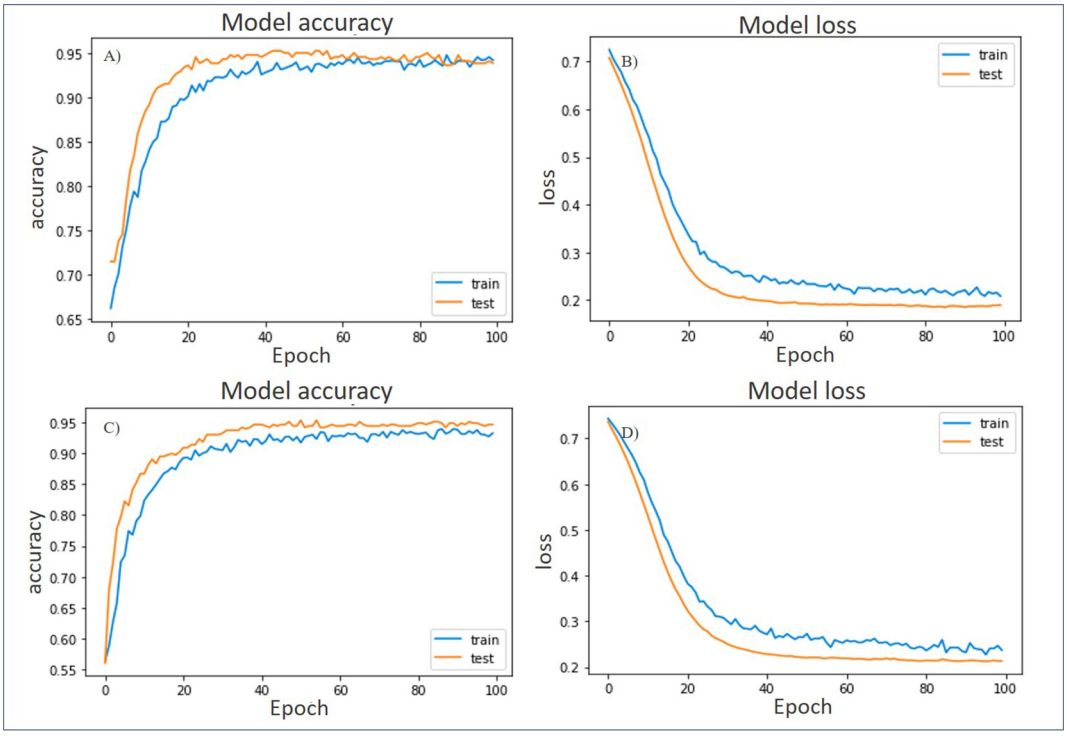

Fig. 9. Accuracy and loss estimation in earthquake induced soil liquefaction hazard prediction. (A) and (B) for 2%, (C) and (D) 10% probability of exceedance rate (ER).

Table 5
Classification results for DNN based earthquake induced LHI prediction.

LHI prediction (2% ER)		Precision	Recall	F1-score	Support
	0	0.934	0.936	0.935	424
	1	0.945	0.943	0.944	494
	accuracy			0.940	918
	macro average	0.939	0.939	0.939	918
	weighted average	0.940	0.940	0.940	918
	Classification accuracy: 0.94%				
LHI prediction (10% ER)		Precision	Recall	F1-score	Support
	0	0.932	0.934	0.932	424
	1	0.943	0.941	0.942	494
	accuracy			0.937	918
	macro average	0.937	0.938	0.937	918
	weighted average	0.938	0.938	0.937	918
	Classification accuracy: 0.93%				

5. Discussion

All the approaches we applied to estimate earthquake-induced soil liquefaction potential and hazard index are reliable (Fig. 4). The assessment of liquefaction potential and hazard involves much difficulty because of the uncertainty in soil characteristics and earthquake occurrence. This study adopted the amplification factor (ratio of response spectra between soil and outcropping rock) of rock types to understand the site classification map. As this study implemented the Vs30 information at bedrock level, PGA was estimated as an earthquake hazard. For moderate earthquakes, PGA is a reasonably good determinant of damage. In severe earthquakes, damage is more often correlated with peak ground velocity. As mentioned before that the Australia has experienced very few moderate events and some low magnitude events therefore PGA was estimated as a ground shaking parameter. Peak ground velocity (PGV) and peak ground displacement (PGD) are important strong ground motion parameters for correlating with damage caused by an earthquake, for the analysis of existing structures and for the design of new structures (Zhu et al., 2015, 2017). However, pseudo-spectral acceleration (PSA) is also used as a parameter for the seismic shaking quantification (Gerstenberger et al., 2007). However, according to the study conducted by Zhu et al. (2017), the PGV performs better than PGA as the shaking intensity parameter. Potential and hazard maps were classified into 4 and 5 classes using a Quantile classification technique, respectively (Jena et al., 2021). The study used quantile classification for training and testing data point creation, and ultimately for final mapping. This study performed liquefaction hazard mapping for the uppermost 30 m of soil. Very-high to high liquefaction hazard can be observed in western coastal parts, along with central and southern Australia. As mentioned earlier, silty sand and sandy sediments are found in the very-high to high hazard locations in Australia. This study found that the possible reasons could be the presence of alluvial layers along with the existence of a shallow groundwater table. However, places where clay content is approximately 0–15%, Vs30 is less than 290 m/s, medium water content 30–80 gm/cm^2, bulk density of 1.4–1.8, and 0–30 m of soil thickness and 5.5 to 6.5 soil pH along with shallow-seated silty sand levels all showed a high potential for liquefaction. This is triggered by the PGA, which varies from 0.003 to 0.48 g for the liquefaction hazard estimation. Hazard areas mostly fall inwards from the coastal locations in western and southern Australia. Our analyses also revealed that the coastal areas of the Spencer Gulf on the south were highly susceptible to liquefaction. When the peak ground acceleration reaches to a_{max} = 0.48 g, much larger areas of Australia would be affected by liquefaction. The low hazard zones identified were characterised by rock (Site Class B, BC, and C) (Dismuke and Mote, 2012). Liquefaction and no-liquefaction case studies by Cetin et al. (2004), Moss et al. (2006), and Idriss and Boulanger (2008) for SPT- and CPT-based assessment, revealed with the minimum CSR7.5 of about 0.05, that the liquefaction was noticed for unconsolidated loose sand, and at approximately 0.1 for medium dense sand. Therefore, a high liquefaction hazard can be expected when CSR7.5 is more than 0.1 and moderate when CSR7.5 is greater than 0.05 but less than 0.1.

A comparative study was done between the PSHA based liquefaction hazard, Geoscience Australia's PGA information-based liquefaction hazard, and a DNNs model based LHI. The results obtained from the first two on 2% and 10% probability of exceedance rate are quite similar to each other. However, the DNNs model-based results show high percentages of areas as high hazard areas. The specific reason could be the use of Geoscience Australia's PGA information based high liquefaction areas as the target of prediction. Still, the performance of the DNNs model is comparable and provides good results. As mentioned earlier, all results are based on global data, while all three approaches provide base maps for an Australian liquefaction study.

Hu et al. (2016) conducted a seismic liquefaction potential assessment on the basis of a Bayesian network constructed using historical information and domain knowledge. Their study results show that the Bayesian network is useful for liquefaction prediction and is feasible in practice. Approximately 90% of their data were correctly classified. Zhang et al., (2021) adopted DNNs to predict soil liquefaction based on shear wave velocity. They achieved peak accuracy values for the training, validation and test sets of 89%, 92% and 93%, respectively. Zhang et al. (2020) applied a constrained backpropagation neural network (C-BPNN) model using the SPT based soil characteristics for liquefaction assessment. Their results recorded 89% accuracy for the study with global applicability. Samui and Sitharam (2011) applied SVM and ANN models for soil liquefaction susceptibility estimation. Their comparative study recorded an accuracy of 94.19% and 88.37% for SVM and ANN, respectively. Kumar et al. (2021) developed a novel methodology for soil liquefaction assessment using deep learning (DL). According to their results, the study achieved 99% and 100% accuracy based on an emotional backpropagation neural network (EmBP) model and deep learning (DL) model, respectively. Xue and Liu (2017) conducted a seismic liquefaction potential study using neural networks. The work implemented BP, GA–BP and PSO–BP models and reported prediction accuracy rates of 94.6%, 95.8% and 97.6%, respectively. No study has been conducted using the GIS thematic layer-based liquefaction potential mapping at a countrywide scale, a feature that makes this study unique. Therefore, PSHA, Geoscience Australian hazard information based and DNNs based liquefaction potential and hazard assessment provide good results, whereas the DNNs achieved 94% and 93% accuracy. Fan et al. (2019) demonstrated that the prediction of earthquake-triggered liquefaction is an earth process that can be used to observe the landscape dynamics. Karpouza and Emvalotis (2019) implemented an integrated hazard evaluation in their study that has the potential to categorize the areas that are threatened either by co-seismic effects and soil liquefaction or integrated occurrence. Therefore, the current study also could be an asset for integrated research and useful for the landscape dynamics observation.

A total of four liquefaction events were experienced in Australia (Dismuke and Mote, 2012). As mentioned earlier, the Southwest Seismic Zone of Meckering in 1968, urban center in Perth, Western Australia and Victoria shows the evidence of liquefaction that is described in detail in Table 6. Therefore, the above information was used to validate the obtained liquefaction hazard maps. Furthermore, the validation was also conducted using the liquefaction hazard maps published by Dismuke and Mote (2012). Although their study was totally based on Vs30 data, however, it shows similar results with our predicted liquefaction hazard maps.

The weakness of the current model deals with the unavailability of country scale borehole data for a geotechnical based liquefaction hazard assessment. Because of the current limitations of our database, this research includes observations of the presence/absence of four paleo liquefaction events and geospatial explanatory variables. Disaggregation of a PSHA is the typical method that should be used to select the magnitude that contributes the most to the ground motion hazard. As a limitation, in Australia, this information is not available. In fact, this is the first study to develop an earthquake-induced soil liquefaction map. This study illustrates the limitations of a country-scale investigation and reinforces the requirement to collect high resolution geophysical and geotechnical data on local scales for earthquake risk assessments.

Table 6
Validation of LHI using the paleo-liquefaction evidence.

Date	Events	Location	Effect	Paleo-liquefaction features	References
10 May 1897	6.5 *Ms*	Southeast of the state at Kingston, Robe and Beachport	Pronounced liquefaction observed.	• The river bank exposed sand, mottled clayey sand, limestone and hematite rubble zone interpreted to be a paleosol, fluvial deposits and modern soil • A shattered dike is still can be seen as a part of paleo-liquefaction	Dismuke and Mote (2012)
06 Feb 1979	6.1 ML	Cadoux, Perth region.	Liquefaction observed in an urban centre located in a large basin in the South West Seismic Zone.	• Found unusual features that might be related to earthquake induced liquefaction in Pleistocene deposits found on the Swan near Courtney Island.	Collins et al. (2004)
14 October 1968	6.8 *Ms*	Western Australian town of Meckering	Induced liquefaction Meckering.	• Liquefaction deposits exposed in the Mortlock River flood plain.	Mosavat et al. (2013)
14 July 1903	5.3 ML	Warrnambool, Victoria	Earthquake shaking is the source of liquefaction.	• Banks of the Goulburn River in Victoria consist of unconsolidated sedimentary deposits near the large scarp in Cadell fault, which originated in the Quaternary period.	Collins et al. (2004)

6. Conclusion

Throughout Australia, areas susceptible to soil liquefaction exist in association with unconsolidated young sediments. In this study, liquefaction is triggered by ground motion levels and earthquake magnitude from the seismological point of view. The PSHA was used to estimate the PGA for 500 and 2500 yr. return periods. The liquefaction hazard maps are intended as an aid to show what might be triggered by events at or above the threshold of M_w 6. Four liquefaction hazard maps were generated with annual exceedance rates of 10% and 2% over a 50-year period, which provide base level tools for evaluating earthquake-induced liquefaction hazard throughout Australia. The derived LPI can be compared to the Australian Site Classification map as a proxy for ground conditions. In practice, the derived LP map is quite similar to the site classification map where low Vs30 Class D, DE, or E fall into the high liquefaction potential zones. For all hazard levels, all the conditioning factors including field-based soil characteristics and groundwater conditions should be used for the improvement of the liquefaction hazard map. At a national scale, the geospatial dataset that includes PGA, Vs30, Soil water content, Clay content and Bulk density and distance to the rivers performs best as a contributing factor to liquefaction hazard. The maps were validated based on the previously published maps and assess the probability and hazard thresholds and the spatial extent of liquefaction. The proposed models are easy to implement for the post-earthquake liquefaction hazard assessment. The geospatial variables can be considered as proxies for three contributing factors such as soil density, saturation, and shaking.

The following conclusions that were made in this study to develop these maps:

(1) Soil that is susceptible to liquefaction was assumed to be present everywhere that was mapped as Classes D, DE, or E sites in previous studies. No conservative assumption was made for the current LPI estimation. Highly susceptible locations can be found in approximately 30% of the study area.
(2) The ground motion variability was based on modern PSHA. However, a threshold magnitude of 6 M_w was assumed for the triggering event for liquefaction, because it is unlikely that earthquake-induced liquefaction is triggered by earthquakes with low magnitudes. LHI varies as 2% (0.032 to 1.9) and 10% (0.008 to 0.5) probability of ER in Australia, respectively.
(3) Several other aspects including local scale geotechnical data can be used for liquefaction micro-zonation using extreme deep learning. The liquefaction hazard maps should always be reality checked against local site and groundwater conditions. Implementation of extreme deep learning and explainable artificial intelligence can be used in future research.

Declaration of Competing Interest

The authors declare that they have no known competing financial interests or personal relationships that could have appeared to influence the work reported in this paper.

Acknowledgment

This research is funded by the Centre for Advanced Modelling and Geospatial Information Systems (CAMGIS), Faculty of Engineering and IT, University of Technology Sydney.

References

Abrahamson, N., Gregor, N., Addo, K., 2016. BC Hydro ground motion prediction equations for subduction earthquakes. Earthq. Spectra 32 (1), 23–44.
Ameri, G., Hollender, F., Perron, V., Martin, C., 2017. Site-specific partially nonergodic PSHA for a hard-rock critical site in southern France: adjustment of ground motion prediction equations and sensitivity analysis. B. Earthq. Eng. 15 (10), 4089–4111.
Andrews, D.C., Martin, G.R., 2000. Criteria for liquefaction of silty soils. In: Proc., 12th World Conf. on Earthquake Engineering. Upper Hutt, New Zealand. NZ Soc. for EQ Engrg, pp. 1–8.
Atkinson, G.M., Boore, D.M., 2003. Empirical ground-motion relations for subduction-zone earthquakes and their application to Cascadia and other regions. Bull. Seismol. Soc. Am. 93 (4), 1703–1729.
Atkinson, G.M., Boore, D.M., 2011. Modifications to existing ground-motion prediction equations in light of new data. Bull. Seismol. Soc. Am. 101 (3), 1121–1135.
Bolton Seed, H., Tokimatsu, K., Harder, L.F., Chung, R.M., 1985. Influence of SPT procedures in soil liquefaction resistance evaluations. J. Geotech. Eng-Asce. 111 (12), 1425–1445.
Boore, D.M., Stewart, J.P., Seyhan, E., Atkinson, G.M., 2014. NGA-West2 equations for predicting PGA, PGV, and 5% damped PSA for shallow crustal earthquakes. Earthq. Spectra 30 (3), 1057–1085.
Bozzoni, F., Bonì, R., Conca, D., Lai, C.G., Zuccolo, E., Meisina, C., 2021. Megazonation of earthquake-induced soil liquefaction hazard in continental Europe. Bull. Earthq. Eng. 19 (10), 4059–4082.
Bray, J.D., Sancio, R.B., Riemer, M.F., Durgunoglu, T., 2004. Liquefaction susceptibility of fine-grained soils. In: Proc. 11th Int. Conf. on Soil Dynamics and Earthquake Engineering and 3rd Int. Conf. on Earthquake Geotechnical Engineering. Stallion Press, Singapore, pp. 655–662.
Campbell, K.W., Bozorgnia, Y., 2014. NGA-West2 ground motion model for the average horizontal components of PGA, PGV, and 5% damped linear acceleration response spectra. Earthq. Spectra 30 (3), 1087–1115.
Castellaro, S., Mulargia, F., Rossi, P.L., 2008. VS30: Proxy for seismic amplification? Seismol. Res. Lett. 79 (4), 540–543.

Cetin, K.O., Seed, R.B., Der Kiureghian, A., Tokimatsu, K., Harder, L.F., Kayen, R.E., 2000. SPT-based probabilistic and deterministic assessment of seismic soil liquefaction initiation hazard. Pacific Earthquake Engineering Research Report No. PEER-2000/05.
Cetin, K.O., Seed, R.B., Der Kiureghian, A., Tokimatsu, K., Harder Jr., L.F., Kayen, R.E., Moss, R.E., 2004. Standard penetration test-based probabilistic and deterministic assessment of seismic soil liquefaction potential. J. Geotech. Geo-Environ. Eng. 130 (12), 1314.
Chakrabortty, P., Nilay, N., Das, A., 2021. Effect of silt content on liquefaction susceptibility of fine saturated river bed sands. Int. J. Civ. Eng. 19 (5), 549–561.
Chandler, A.M., Pappin, J.W., Coburn, A.W., 1991. Vulnerability and seismic risk assessment of buildings following the 1989 Newcastle, Australia earthquake. Bull. NZSEE 24 (2), 116–138.
Chiou, B.S.J., Youngs, R.R., 2014. Update of the Chiou and Youngs NGA model for the average horizontal component of peak ground motion and response spectra. Earthq. Spectra 30 (3), 1117–1153.
Clark, D., McPherson, A., Collins, C., 2010. M_{max} estimates for the Australian stable continental region (SCR) derived from palaeoseismicity data. Proceedings of the 2010 AEES Conference.
Collins, C., Cummins, P., Clark, D., Tuttle, M., Van Arsdale, R., 2004. Paleoliquefaction studies in Australia to constrain earthquake hazard estimates. In Proceedings of 2004 NZSEE Conference, Rotorua, 19-24 March 2004, Paper (Vol. 50).
Cornell, C.A., 1968. Engineering seismic risk analysis. Bull. Seismol. Soc. Am. 58 (5), 1583–1606.
Dismuke, T.M.J., Mote, J.N., 2012. Liquefaction hazard maps for Australia. Paper of all World Conferences on Earthquake Engineering. https://www.iitk.ac.in/nicee/wcee/article/WCEE2012_3982.pdf (Accessed 12 March 2021).
Fan, X., Scaringi, G., Korup, O., West, A.J., van Westen, C.J., Tanyas, H., Hovius, N., Hales, T.C., Jibson, R.W., Allstadt, K.E., Zhang, L., 2019. Earthquake-induced chains of geologic hazards: Patterns, mechanisms, and impacts. Rev. Geophys. 57 (2), 421–503.
Farrokhzad, F., Choobbasti, A.J., Barari, A., 2012. Liquefaction microzonation of Babol city using artificial neural network. J. King Saud Univ. Sci. 24 (1), 89–100.
Fitzsimons, I.C.W., 2003. Proterozoic basement provinces of southern and southwestern Australia, and their correlation with Antarctica. Geol. Soc. Spec. Pub. 206 (1), 93–130.
Gerstenberger, M.C., Worden, C.B., Wald, D.J., 2007. A probabilistic relationship between ground shaking parameters and MMI based on felt report data. Proceedings of the New Zealand Society of Earthquake EngIneerIng Technical Conference 2007.
Glorot, X., Bordes, A., Bengio, Y., 2011. June. Deep sparse rectifier neural networks. In: Proceedings of the Fourteenth AISTATS 2021. JMLR Workshop and Conference Proceedings, pp. 315–323.
Goh, A.T., 1994. Seismic liquefaction potential assessed by neural networks. J. Geotech. Eng-ASCE. 120 (9), 1467–1480.
Goh, A.T., Goh, S.H., 2007. Support vector machines: their use in geotechnical engineering as illustrated using seismic liquefaction data. Comput. Geotech. 34 (5), 410–421.
Gülerce, Z., Kargoığlu, B., Abrahamson, N.A., 2016. Turkey-adjusted NGA-W1 horizontal ground motion prediction models. Earthq. Spectra 32 (1), 75–100.
Gutenberg, B., Richter, C.F., 1956. Earthquake magnitude, intensity, energy, and acceleration (Second paper). Bull. Seismol. Soc. Am. 46 (2), 105–145.
Hu, J.L., Tang, X.W., Qiu, J.N., 2016. Assessment of seismic liquefaction potential based on Bayesian network constructed from domain knowledge and history data. Soil. Dyn. Earthq. Eng. 89, 49–60.
Icold, 1989. Selecting seismic parameters for large dams. ICOLD Bulletin No 72.
Idriss, I.M., 1990. Response of soft soil sites during earthquakes. Proc. HB Seed Memorial Symp. 2, 273–289.
Idriss, I.M., Boulanger, R.W., 2008. Soil Liquefaction During Earthquake, Earthquake Engineering Research Institute. EERI Publication MNO-12.
Ishihara, K., 1977. Simple method of analysis for liquefaction of sand deposits during earthquakes. Soils Found. 17 (3), 1–17.
Iwasaki, T., Arakawa, T., Tokida, K.I., 1984. Simplified procedures for assessing soil liquefaction during earthquakes. Soil Dynam. Earthq. Engng. 3 (1), 49–58.
Jena, R., Pradhan, B., Naik, S.P., Alamri, A.M., 2021. Earthquake risk assessment in NE India using deep learning and geospatial analysis. Geosci. Front. 12, (3). https://doi.org/10.1016/j.gsf.2020.11.007 101110.
Joyner, W.B., Boore, D.M., 1981. Peak horizontal acceleration and velocity from strong-motion records including records from the 1979 Imperial Valley, California, earthquake. Bull. Seismol. Soc. Am. 71 (6), 2011–2038.
Juang, C.H., Chen, C.J., Jiang, T., Andrus, R.D., 2000. Risk-based liquefaction potential evaluation using standard penetration tests. Can. Geotech. J. 37 (6), 1195–1208.
Karpouza, M., Chousianitis, K., Bathrellos, G.D., Skilodimou, H.D., Kaviris, G., Antonarakou, A., 2021. Hazard zonation mapping of earthquake-induced secondary effects using spatial multi-criteria analysis. Nat. Hazards 109 (1), 637–669.
Karpouza, E., Emvalotis, A., 2019. Exploring the teacher-student relationship in graduate education: a constructivist grounded theory. Teaching in Higher Education 24 (2), 121–140.
Karthikeyan, J., Kim, D., Aiyer, B.G., Samui, P., 2013. SPT-based liquefaction potential assessment by relevance vector machine approach. Eur. J. Environ. Civ. En. 17 (4), 248–262.
Khan, M.M., Kumar, G.K., 2018. Statistical completeness analysis of seismic data. J. Geol. Soc. India 91 (6), 749–753.
Kumar, D., Samui, P., Kim, D., Singh, A., 2021. A novel methodology to classify soil liquefaction using deep learning. Geotech. Geol. Eng. 39 (2), 1049–1058.
Lee, C.Y., Chern, S.G., 2013. Application of a support vector machine for liquefaction assessment. J. Mar. Sci. Technol. 21 (3), 318–324.
Liao, S.S., Veneziano, D., Whitman, R.V., 1988. Regression models for evaluating liquefaction probability. J. Geotech. Eng-ASCE. 114 (4), 389–411.
Lilley, F.E.M., Wang, L.J., Chamalaun, F.H., Ferguson, I.J., 2003. Carpentaria electrical conductivity anomaly, Queensland, as a major structure in the Australian Plate. Special Papers-Geological Society of America, 141–156.
Lin, A., Wotherspoon, L., Blake, D., Bradley, B., Motha, J., 2020. Liquefaction exposure and impacts across New Zealand State Highways. In: NZGS Symposium 2021, Dunedin, New Zealand, pp. 1–9.
Liu, Z., Tesfamariam, S., 2012. Prediction of lateral spread displacement: data-driven approaches. Bull. Earthq. Eng. 10 (5), 1431–1454.
McPherson, A., Hall, L., 2013. Site classification for earthquake hazard and risk assessment in Australia. Bull. Seismol. Soc. Am. 103 (2A), 1085–1102.
Meinesz, F.V., 1947. Shear patterns of the Earth's crust. Eos, Trans. Am. Geophys. Union 28 (1), 1–61.
Mitchell, P., Moore, C., 2007. Difficulties in assessing liquefaction potential from conventional field testing. In The AEES Conferences.
Mosavat, N., Oh, D.E., Chai, D.G., 2013. Liquefaction risk potential of road foundation in the Gold Coast Region, Australia. Electron. J. Geotech. Eng. 18, 1493–1504.
Moss, R., Seed, R., Kayen, R., Stewart, J., Kiureghian, A., Cetin, K.E.M.A.L., 2006. CPT-based probabilistic and deterministic assessment of in situ seismic soil liquefaction potential. J. Geotech. Geo-Environ. Eng. 132 (8), 1032–1051.
Mote, T.I., Dismuke, J.N., 2011. Screening-Level Liquefaction Hazard Maps for Australia. AEES.
Mughieda, O., Bani-Hani, K., Safieh, B., 2009. Liquefaction assessment by artificial neural networks based on CPT. Int. J. Geotech. Eng. 3 (2), 289–302.
Murugan, P., 2018. Implementation of deep convolutional neural network in multi-class categorical image classification. arXiv:1801.01397.
Nath, S.K., Thingbaijam, K.K.S., 2012. Probabilistic seismic hazard assessment of India. Seismol. Res. Lett. 83 (1), 135–149.
Ollier, C.D., 1979. Evolutionary geomorphology of Australia and Papua: New Guinea. T. I. Brit. Geogr., 516–539
Olson, S.M., Stark, T.D., 2003. Yield strength ratio and liquefaction analysis of slopes and embankments. J. Geotech. Geoenviron. 129 (8), 727–737.
Pal, M., 2006. Support vector machines-based modelling of seismic liquefaction potential. Int. J. Numer. Anal. Met. 30 (10), 983–996.
Poulos, S.J., Castro, G., France, J.W., 1985. Liquefaction evaluation procedure. J. Geotech. Eng-ASCE. 111 (6), 772–792.
Quigley, M.C., Cupper, M.L., Sandiford, M., 2006. Quaternary faults of south-central Australia: palaeoseismicity, slip rates and origin. Aust. J. Earth Sci. 53 (2), 285–301.
Ramakrishnan, D., Singh, T.N., Purwar, N., Barde, K.S., Gulati, A., Gupta, S., 2008. Artificial neural network and liquefaction susceptibility assessment: a case study using the 2001 Bhuj earthquake data, Gujarat, India. Computat. Geosci. 12 (4), 491–501.
Samui, P., Sitharam, T.G., 2011. Machine learning modelling for predicting soil liquefaction susceptibility. Nat. Hazard. Earth. Sys. 11 (1), 1–9.
Seed, H.B., Idriss, I.M., 1971. Simplified procedure for evaluating soil liquefaction potential. J. Soil Mech. Found. 97 (9), 1249–1273.
Seed, H.B., Woodward, R.J., Lundgren, R., 1964. Fundamental aspects of the Atterberg limits. J. Soil Mech. Found. 90 (6), 75–106.
Seed, H.B., Idriss, I.M., Arango, I., 1983. Evaluation of liquefaction potential using field performance data. J. Geotech. Eng-ASCE. 109 (3), 458–482.
Semple, R., 2013. Problems with liquefaction criteria and their application in Australia. Aust. Geomech. J. 48 (3), 15–34.
Spec, G.S.A., Pap, G.S.A.S., 2003. Crustal thickness patterns in the Australian continent. Evolution and dynamics of the Australian Plate 372, p.121.
State Infrastructure Commission, 1974. Code for Seismic Design of Industrial and Civil Buildings, TJ 11-74. Beijing, China Building Industry Press (in Chinese).
Tallett-Williams, S., 2017. Site classification for seismic hazard assessment in low seismicity regions. Ph.D. thesis, Imperial College London, 291 pp.
Tatsuoka, F., Iwasaki, T., Tokida, K.I., Yasuda, S., Hirose, M., Imai, T., Kon-No, M., 1980. Standard penetration tests and soil liquefaction potential evaluation. Soils Found. 20 (4), 95–111.
Trifunac, M.D., 2016. Site conditions and earthquake ground motion–A review. Soil Dyn. Earthq. Eng. 90, 88–100.
Wills, C.J., Petersen, M., Bryant, W.A., Reichle, M., Saucedo, G.J., Tan, S., Taylor, G., Treiman, J., 2000. A site-conditions map for California based on geology and shear-wave velocity. Bull. Seismol. Soc. Am. 90 (6B), S187–S208.
Wotherspoon, L.M., Pender, M.J., Orense, R.P., 2012. Relationship between observed liquefaction at Kaiapoi following the 2010 Darfield earthquake and former channels of the Waimakariri River. Eng. Geol. 125, 45–55.
Xu, L., Ren, J.S., Liu, C., Jia, J., 2014. Deep convolutional neural network for image deconvolution. Adv. Neur. In. 27, 1790–1798.
Xue, X., Liu, E., 2017. Seismic liquefaction potential assessed by neural networks. Environ. Earth Sci. 76 (5), 192.
Zhang, W., Goh, A.T., 2016. Evaluating seismic liquefaction potential using multivariate adaptive regression splines and logistic regression. Geomech. Eng. 10 (3), 269–284.
Zhang, W., Goh, A.T., 2018. Assessment of soil liquefaction based on capacity energy concept and back-propagation neural networks. Integr. Disaster Sci. Manage., 41–51
Zhang, L., Tan, J., Han, D., Zhu, H., 2017. From machine learning to deep learning: progress in machine intelligence for rational drug discovery. Drug Discov. Today 22 (11), 1680–1685.

Zhang, Y., Wang, R., Zhang, J.M., Zhang, J., 2020. A constrained neural network model for soil liquefaction assessment with global applicability. Front. Struct. Civ. Eng. 14 (5), 1066–1082.
Zhang, Y., Xie, Y., Zhang, Y., Qiu, J., Wu, S., 2021. The adoption of deep neural network (DNN) to the prediction of soil liquefaction based on shear wave velocity. Bull. Eng. Geol. Environ., 1–8
Zhang, J., Zhang, L.M., Huang, H.W., 2013. Evaluation of generalized linear models for soil liquefaction probability prediction. Environ. Earth Sci. 68 (7), 1925–1933.
Zhao, J.X., Zhang, J., Asano, A., Ohno, Y., Oouchi, T., Takahashi, T., Ogawa, H., Irikura, K., Thio, H.K., Somerville, P.G., Fukushima, Y., 2006. Attenuation relations of strong ground motion in Japan using site classification based on predominant period. Bull. Seismol. Soc. Am. 96 (3), 898–913.
Zhu, J., Daley, D., Baise, L.G., Thompson, E.M., Wald, D.J., Knudsen, K.L., 2015. A geospatial liquefaction model for rapid response and loss estimation. Earthq. Spectra 31 (3), 1813–1837.
Zhu, J., Baise, L.G., Thompson, E.M., 2017. An updated geospatial liquefaction model for global application. Bull. Seismol. Soc. Am. 107 (3), 1365–1385.